

REPORTS

(derivative-like) and 2.7 eV (absorption band), which are similar to those in disordered films (14), the RR P3HT EA spectrum also contains strong oscillation with zero crossing at 2.75 eV (Fig. 4). Such oscillation was previously seen in α -sexithienyl microcrystallites and analyzed in terms of a charge-transfer exciton near the continuum level (29). This may be a prerequisite for the formation of Franz-Keldysh band-edge oscillation, such as in EA of single-crystal polydiacetylene (30). We also found that this oscillation gradually disappears upon aging of the film, due to reduced electron coherence caused by the oxygen attack on the polymer chains (Fig. 4).

In conclusion, we studied and compared long-lived photoexcitations in RR and RRa P3AT films. In RR P3AT films, where lamellae are formed, the increased interplane interchain interaction, t_{\perp} delocalizes the traditional 1D charged polarons onto adjacent chains, acquiring 2D electronic properties. The most prominent optical signature of the delocalized polaron excitation is a strong red-shifted absorption band in the mid-IR range (DP_1) that may be used to directly measure t_{\perp} in polymer films by optical means. In addition, the relatively weak transitions of the delocalized polaron excitation in the visible and NIR spectral range may help to achieve laser action in nanocrystalline polymer devices using current injection, by reducing the optical loss at wavelengths near the exciton-stimulated emission band; so far, this has been an acute problem in the field of plastic lasers. Moreover, although the absorption spectrum of delocalized polaron excitation approaches that of free carriers in more conventional 3D semiconductors, it still contains a low-frequency spectral gap of ~ 60 meV, which is due to the polaronic relaxation and which may be reflected in the relatively low carrier mobility in these films. A further increase of t_{\perp} will close the gap, destabilize the delocalized polaron excitation, and enhance carrier mobility by additional orders of magnitudes. All organic electronic and optoelectronic applications of nanocrystalline π -conjugated polymers may then become a reality.

References and Notes

- X. Peng, G. Horovitz, D. Fichou, F. Garnier, *Appl. Phys. Lett.* **57**, 2013 (1990); *Adv. Mater.* **2**, 592 (1990).
- B. Serbet *et al.*, *Adv. Mater.* **5**, 461 (1993); W. Porzio, S. Destri, M. Mascherpa, S. Brucker, *Acta Polym.* **44**, 266 (1993).
- F. Biscarini *et al.*, *Phys. Rev. B* **52**, 14868 (1995).
- D. Fichou *et al.*, *Adv. Mater.* **8**, 500 (1996).
- P. Lane *et al.*, *Chem. Phys.* **210**, 229 (1996); P. Lane *et al.*, *Chem. Phys.* **227**, 57 (1998); G. Lanzani *et al.*, *Phys. Rev. Lett.* **79**, 3066 (1997).
- T. A. Chen, X. Wu, R. D. Rieke, *J. Am. Chem. Soc.* **117**, 233 (1995); T. J. Prosa, M. J. Winokur, R. D. McCullough, *Macromolecules* **29**, 3654 (1996).
- R. D. McCullough, *Adv. Mater.* **10**, 93 (1998).
- Z. Bao, A. Dodabalapur, A. J. Lovinger, *Appl. Phys. Lett.* **69**, 4108 (1996).
- H. Sirringhaus, N. Tessler, R. H. Friend, *Science* **280**, 1741 (1998); A. Dodabalapur *et al.*, *Appl. Phys. Lett.* **73**, 142 (1998).
- G. Horovitz, *Adv. Mater.* **10**, 365 (1998).
- H. Sirringhaus *et al.*, *Nature* **401**, 685 (1999).
- Z. V. Vardeny and X. Wei, in *Handbook of Conducting Polymers*, T. A. Skotheim, R. L. Elsenbaumer, J. R. Reynolds, Eds. (Dekker, New York, ed. 2, 1997), chap. 22.
- M. Deussen and H. Bassler, *Synth. Met.* **54**, 49 (1993).
- M. Liess *et al.*, *Phys. Rev. B* **56**, 15712 (1997).
- K. Fesser, A. R. Bishop, D. K. Campbell, *Phys. Rev. B* **27**, 4804 (1983).
- B. Horovitz, *Solid State Commun.* **41**, 729 (1982).
- E. Ehrenfreund, Z. Vardeny, O. Brafman, B. Horovitz, *Phys. Rev. B* **36**, 1535 (1987).
- Y. N. Garstein and A. A. Zakhidov, *J. Mol. Electron.* **3**, 163 (1987); H. A. Mizes and E. M. Conwell, *Phys. Rev. B* **50**, 11243 (1994).
- D. Emin, *Phys. Rev. B* **33**, 3973 (1986).
- Yu. N. Garstein and A. A. Zakhidov, *Solid State Commun.* **60**, 105 (1986); *Solid State Commun.* **62**, 213 (1987).
- D. Baeriswyl and K. Maki, *Synth. Met.* **28**, D507 (1989); *Synth. Met.* **41–43**, 3585 (1991).
- P. Vogl and D. K. Campbell, *Phys. Rev. Lett.* **62**, 2012 (1989); *Phys. Rev. B* **41**, 12797 (1990).
- H. A. Mizes and E. M. Conwell, *Phys. Rev. Lett.* **70**, 1505 (1993).
- J. Blackman and M. K. Sabra, *Phys. Rev. B* **47**, 15437 (1993).
- Y. N. Gartstein and A. A. Zakhidov, *Synth. Met.* **28**, D501 (1989); *Synth. Met.* **41–43**, 3649 (1991).
- M. G. Harrison, R. H. Friend, F. Garnier, A. Yassar, *Synth. Met.* **67**, 215 (1994).
- M. J. Rice, *Phys. Rev. Lett.* **37**, 36 (1976); B. Horovitz, H. Gutfreund, M. Weger, *Phys. Rev. B* **17**, 2796 (1978).
- The interchain coupling constant t_{\perp} may not be related to the in-plane interchain distance a (Fig. 1C) in a simple way. In fact, it may be a complicated function of n , as was previously realized in the field of charge-transfer salts.
- L. M. Blinov *et al.*, *Chem. Phys. Lett.* **232**, 401 (1995).
- L. Sebastian and G. Weiser, *Phys. Rev. Lett.* **46**, 1156 (1981).
- We thank H. Sirringhaus for sending us a preprint of his work (17) before publication and S. Mazumdar for useful discussions. Supported in part by NSF grant DMR 97-32820 and U.S. Department of Energy grant ER 45490. R.O. acknowledges funding from the Swedish Academy for Engineering Sciences in Finland, the Neste Foundation, and the Ehrnrooth Foundation.

9 September 1999; accepted 9 December 1999

Cool Glacial Temperatures and Changes in Moisture Source Recorded in Oman Groundwaters

Constanze E. Weyhenmeyer,¹ Stephen J. Burns,¹
H. Niklaus Waber,¹ Werner Aeschbach-Hertig,² Rolf Kipfer,²
H. Hugo Loosli,³ Albert Matter¹

Concentrations of atmospheric noble gases (neon, argon, krypton, and xenon) dissolved in groundwaters from northern Oman indicate that the average ground temperature during the Late Pleistocene (15,000 to 24,000 years before present) was $6.5^{\circ} \pm 0.6^{\circ}\text{C}$ lower than that of today. Stable oxygen and hydrogen isotopic groundwater data show that the origin of atmospheric water vapor changed from a primarily southern, Indian Ocean source during the Late Pleistocene to a dominantly northern, Mediterranean source today. The reduced northern water vapor source is consistent with a drier Last Glacial Maximum through much of northern Africa and Arabia.

Large discrepancies exist in estimates of tropical glacial-interglacial temperature changes during the Pleistocene-Holocene transition (1–4). These discrepancies are an obstacle to producing predictive general circulation models (GCMs) of climate. Reconstructions of sea surface temperature (SST) based on transfer function analyses of planktonic foraminiferal assemblages originally indicated that there was less than a 2°C change in tropical SST between the Last Glacial Maximum (LGM) and the Holocene (5–8). Alkenones in deep-sea sediments suggest only a slightly larger glacial-interglacial increase in SST of 2° to 3°C (9, 10). More recent studies of Sr/Ca ratios and $\delta^{18}\text{O}$ (11) records of corals, however, indicate that

tropical SST was as much as 5°C cooler during the LGM than today (12). The coral records are more consistent with available continental paleoclimate studies on vegetation, snow lines, tropical ice cores, and groundwater, which indicate an even larger tropical Pleistocene-Holocene temperature increase of 5° to 8°C (13–20).

SST maps for the LGM are commonly used as boundary conditions for atmospheric circulation models of climate change or as an independent test for GCM simulations (2, 3). Atmospheric circulation models that use CLIMAP SST distributions as boundary conditions generally predict little continental glacial-interglacial temperature changes for tropical regions (2), which is inconsistent with most available geological proxies. More recent simulations with modified SST fields (3) and coupled atmosphere-ocean GCMs (4) that include ocean dynamics (e.g., thermohaline circulation

¹Institute of Geology, University of Bern, CH-3012 Bern, Switzerland. ²Environmental Physics, EAWAG/ETH, CH-8600 Dübendorf, Switzerland. ³Institute of Physics, University of Bern, CH-3012 Bern, Switzerland.

REPORTS

and upwelling) predict substantially larger tropical glacial-interglacial temperature changes, with temperature increases of up to 5° to 7°C for the continental interiors of the tropics, although with considerable spatial variability. Because the magnitude to which the tropics cooled during the LGM has important implications for their role in global climatic changes, resolving the discrepancies between various computer simulations and geological proxies is a key issue in paleoclimate research. At present, the preponderance of geological data indicating substantially cooler tropical and subtropical temperatures during the LGM come from the Americas, an area that is strongly influenced by changes in North Atlantic circulation and particularly in North Atlantic Deep Water formation. More paleotemperature records from different geographical regions are needed to assess the magnitude and global extent of glacial-interglacial temperature changes.

We present a paleoclimate record from Oman, southeastern Arabia, which extends the global tropical paleotemperature database to an area lacking any previous continental temperature record for the Late Pleistocene. Paleotemperature estimates are based on measurements of Ne, Ar, Kr, and Xe dissolved in ¹⁴C-dated groundwater (21). Stable isotope analyses of the groundwater ($\delta^{18}\text{O}$ and $\delta^2\text{H}$) (22) yield additional information on the Late Pleistocene moisture sources and tropical atmospheric circulation (23). The coastal aquifer of the Al Khwad Fan, located in northern Oman (23°30'N, 58°E) (Fig. 1), covers an area of about 250 km². The aquifer consists of an alluvial, ophiolitic gravel sequence greater than 400 m thick, underlain by the Semail ophiolite. At present, recharge in the catchment occurs mainly during the winter months as a result of Mediterranean frontal systems passing through the area from the northwest. A secondary source is local convective storm cells that form during the very hot summers. Tropical cyclones occasionally approach the area, originating either in the southeastern Arabian Sea or in the Bay of Bengal (24, 25). Because of the strong offshore monsoonal airstream that parallels the southeastern Arabian coast during the summer and winter, however, these southern air masses normally do not reach the Arabian coast and thus do not contribute substantially to the present-day recharge. The southwest summer monsoon that accounts for most of the precipitation in southern Oman also does not reach the study area in northern Oman.

Three aquifers can be distinguished in the Al Khwad Fan catchment on the basis of geochemical and isotopic data from more than 50 wells: a deep aquifer below 300-m depth containing old groundwater, an intermediate aquifer between 50 and 300 m containing mixed groundwater, and a shallow aquifer filled with

recently infiltrated groundwater (26). The low ¹⁴C activities recorded for the deep groundwater indicate infiltration during the Late Pleistocene sometime around the LGM [21,000 years before present (yr B.P.)]. Calculated ¹⁴C residence times of the deep groundwater range from 15,000 to 24,000 yr B.P. when corrected for carbonate chemistry (27) and changes in atmospheric ¹⁴C concentrations through time (28). Although hydrologically heterogeneous, the Al Khwad Fan catchment is geochemically rather homogeneous with a dominant ophiolitic host-rock composition (bedrock and gravels) so that all groundwaters have very low concentrations of calcium and dissolved inorganic carbon. As a result, the modeled ¹⁴C residence times were found to be relatively insensitive to the choice of correction model and to changes in input parameters (e.g., soil CO₂), yielding an overall uncertainty of individual ages of ± 1000 years. Infiltration within the past 50 years is indicated for groundwater samples from the shallow aquifer, which are all tritium (³H) bearing with associated ¹⁴C activities close to modern atmospheric input. Chemical and isotopic data of groundwater samples from the intermediate aquifer indicate complex mixtures of Late Pleistocene and modern groundwater together with variable, but generally small (<5%) amounts of seawater from the coastal saline intrusion wedge.

Eleven wells were selected and resampled for noble gas analyses, on the basis of the groundwater chemistry and isotope data. Noble gas temperatures (NGT) were calculated from the measured concentrations of Ne, Ar, Kr, and Xe dissolved in the groundwater with a weighted least-square fitting technique and a model for excess air fractionation (29).

The average NGT calculated for the three Holocene samples from the upper aquifer is $33.5 \pm 1.7^\circ\text{C}$ (30). These estimated infiltration temperatures closely agree with measured groundwater temperatures (30) and the average annual ground temperature at the water table ($33^\circ \pm 0.3^\circ\text{C}$) as determined from borehole temperature measurements from more than 50

wells in the study area (26). The three Pleistocene groundwater samples yield consistent NGTs between 26° and 27°C, with an average of $26.6^\circ \pm 0.6^\circ\text{C}$, about $6.5^\circ \pm 0.6^\circ\text{C}$ lower than the average annual ground temperature at the water table today (Fig. 2).

A glacial-interglacial temperature increase of $6.5^\circ \pm 0.6^\circ\text{C}$ lies in the upper range of previously published estimates from the tropical regions. However, several continental records, mostly from the Americas, indicate a tropical and subtropical glacial-interglacial temperature increase of similar magnitude. Pollen records from Mexico, Panama, and Colombia, for example, suggest a temperature increase of 5° to 8°C, and changes in vegetation zones in the Colombian and Ecuadorian Andes indicate a warming of similar magnitude if today's lapse rate is used for temperature conversions (13, 15, 16). Noble gas studies of groundwater from tropical Brazil, Namibia, and Nigeria also support a glacial-interglacial temperature increase of 5° to 8°C (19, 20). Although, there has been recent discussion of the exact temperature conversion of stable isotope records from tropical ice cores (18), records from the equatorial Andes provide additional evidence for substantially cooler tropical temperatures during the Late Pleistocene (17). Because most continental paleotemperature records come from tropical Central and South America, the question remains of whether such large glacial-interglacial temperature change was also the case for tropical continental regions more distant from the North Atlantic region. The Oman record provides evidence for a large continental glacial-interglacial temperature difference outside the Americas, thus adding support for a global extent of substantially cooler tropical and subtropical temperatures around the LGM.

The only other available Late Pleistocene temperature estimates for the Arabian region come from studies of sediments from the Indian Ocean. These studies suggest that during the LGM, mean annual SST for the Bay of Bengal

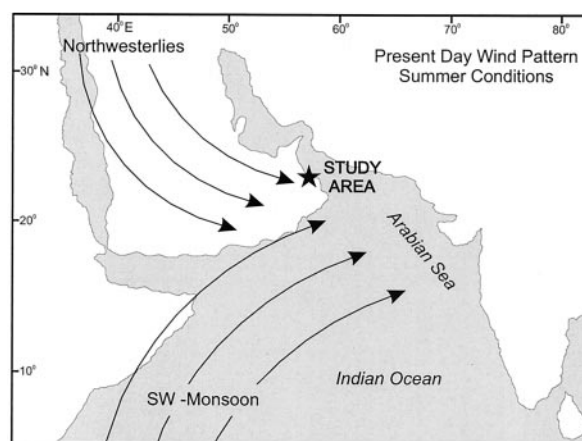


Fig. 1. Map showing the location of the Al Khwad Fan aquifer, including a generalized sketch of the present-day wind pattern during summer (July and August). The southwest (SW) monsoon reaches only the southern coastal areas of Oman and does not affect the northern regions. Water vapor carried to the study area by the northwesterly winds is the main source for present-day recharge.

REPORTS

was only 1° to 2°C lower than modern values, whereas the Arabian Sea was interpreted to be as warm or even warmer during the LGM than it is today (8, 10). Such a large discrepancy between our continental and the marine records appears at first improbable. Marine records from the Arabian Sea, however, are strongly influenced by upwelling, induced by the southwest summer monsoon (8, 31–33). Upwelling brings cold, nutrient-rich deep water to the surface, resulting in a cooling of several degrees. During summer, long-term average SST is as low as 23° to 24°C along the coasts of Africa and Arabia, as compared with 27° to 28°C in areas that are not affected by upwelling (24). It is generally thought that as a result of a southward movement of the Intertropical Convergence Zone (ITCZ), the summer southwest monsoon was weakened whereas the dry winter northeast monsoon was intensified during the

LGM (8, 31, 32). As a result, upwelling off the coasts of Oman and Somalia was presumably substantially reduced during the Late Pleistocene, resulting in relatively warmer SST in the western Arabian Sea. Thus, the glacial-interglacial changes in upwelling intensity would dampen the overall glacial-interglacial temperature change in marine records from parts of the Arabian Sea. Although changes in upwelling intensity alone cannot completely resolve the discrepancies between marine and continental records of the Arabian Sea region, such changes in ocean dynamics need to be considered when comparing the different climate change proxies from this area.

Results from stable isotope analyses from the Al Khwad Fan groundwaters suggest that, in addition to the general cooling during the Late Pleistocene, there was also a change in the source of water vapor recharging the

aquifer. Late Pleistocene groundwater samples from the Al Khwad Fan are depleted in deuterium by several per mil but show no substantial change in $\delta^{18}\text{O}$ when compared with modern infiltration waters (34). Thus, the Pleistocene groundwater samples do not fall on the modern local groundwater line (Fig. 3). This isotopic shift could theoretically be the result of either of two processes: increased evaporation or changes in the source of local water vapor (23). Because concentrations of conservative elements (i.e., Cl, Na, and Br) in the Pleistocene groundwater samples are very similar to those in the Holocene groundwater, changes in evaporation rates are an unlikely explanation for the observed isotopic offset. Rather, a change in the dominant water vapor source is the most likely cause. Previous work on rainwater allowed us to identify two separate local meteoric water lines for northern Oman (26). These meteoric water lines reflect two different principal water vapor sources for precipitation in the area: a northern, Mediterranean vapor source and a southern, Indian Ocean source. The Late Pleistocene groundwater samples from the Al Khwad Fan fall directly on the southern local meteoric water line (Fig. 3), indicating a dominantly southern, Indian Ocean water vapor source for groundwater recharge during the Late Pleistocene. Because during the LGM the ITCZ was farther south than it is today, the study area was presumably not affected by the southwest monsoon, and thus an intensification of precipitation from this southern water vapor source appears unlikely. Instead, the observed isotope shift in the Late Pleistocene groundwater samples is probably the result of a weakening or disappearance of the northern water vapor source that recharges the aquifer today. A reduced northern water vapor source during the Late Pleistocene is consistent with continental groundwater, lake, and pollen records, all of which suggest that the LGM was substantially drier through much of Arabia, Africa, and southern Europe compared with the present day (20, 35–37). As a result of a drier LGM climate over the northwestern continental regions, the northwestern air masses that provide most of the modern-day precipitation to northern Oman would not have carried enough moisture to produce substantial amounts of precipitation during this time.

Final questions concerning Late Pleistocene groundwater in the Al Khwad Fan are why the aquifer was recharged during a drier climate period and why the aquifer was not flushed during the subsequent Holocene wet period that occurred throughout Africa, Arabia, and Asia between about 6000 and 10,000 yr B.P. (35–38). A change in sea level is a potential mechanism for preservation of the deep coastal groundwater. During the LGM, sea level was about 120 m below that of the present (39),

Fig. 2. Calculated noble gas temperatures versus corrected ^{14}C groundwater ages for the three different aquifers. Groundwater samples from the intermediate aquifer are a mixture between modern and Pleistocene groundwater, as determined from the groundwater chemistry. The solid line indicates the present-day average annual ground temperature at the water table, $33^\circ \pm 0.3^\circ\text{C}$. Data point labels correspond to well identification numbers (30).

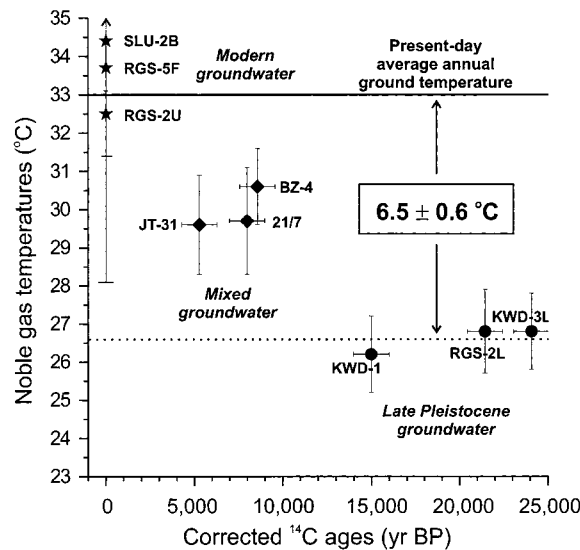
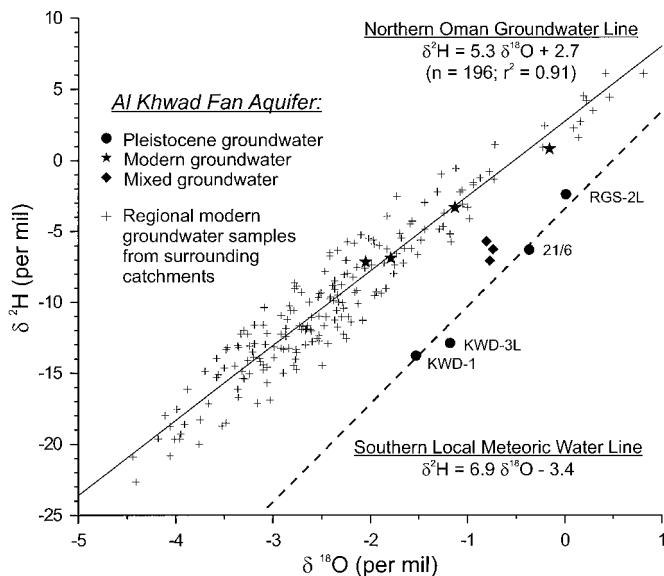


Fig. 3. Cross plot of $\delta^{18}\text{O}$ versus $\delta^2\text{H}$. The southern local meteoric water line (dashed line) was determined from measurements of precipitation from southern tropical cyclones reaching the study area occasionally (26). The crosses represent data from 196 Late Holocene (<1000 years) groundwater samples from the Al Khwad Fan and surrounding catchments, providing the northern Oman groundwater line as a reference for modern infiltrated groundwater in the area. The range of isotope values reflects the range of recharge altitude between 0 and 2000 meters above sea level, with the more depleted values indicating high-altitude recharge.



resulting in substantially increased hydraulic gradients on the coastal plain. The more distant outlets of the groundwater flow, combined with greater hydraulic gradients, likely resulted in much deeper circulation of fresh water than at present. When sea level rose during the Pleistocene-Holocene transition, hydraulic gradients greatly decreased, and the Pleistocene groundwater in the lower parts of the aquifer was disconnected from the active flow system above. The reduced hydraulic gradients and resulting shallower groundwater circulation also prevented flushing of this part of the aquifer during the subsequent early to mid Holocene wet period.

References and Notes

1. E. Bard, *Science* **284**, 1133 (1999).
2. J. E. Kutzbach and P. J. Guetter, *J. Atmos. Sci.* **43**, 1726 (1986); A. J. Broccoli and S. Manabe, *Clim. Dyn.* **1**, 87 (1987).
3. R. S. Webb, D. H. Rind, S. J. Lehman, R. J. Healy, D. Sigman, *Nature* **385**, 695 (1997); S. W. Hostetler and A. C. Mix, *Nature* **399**, 673 (1999).
4. A. B. G. Bush and S. G. H. Philander, *Science* **279**, 1341 (1998); A. Ganopolski, S. Rahmstorf, V. Petoukhov, M. Claussen, *Nature* **391**, 351 (1998).
5. CLIMAP: Climate/Long-Range Investigation, Mapping and Prediction Project Members, *Geol. Soc. Am. Map Chart Ser.* **36** (1981); *Science* **191**, 1131 (1976).
6. R. Thunell, D. Anderson, D. Gellar, Q. Miao, *Quat. Res.* **41**, 255 (1994); L. D. Stott and C. M. Tang, *Paleoceanography* **11**, 37 (1996).
7. W. Broecker, *Quat. Res.* **26**, 121 (1986).
8. J. C. Duplessy, *Nature* **295**, 494 (1982); W. L. Prell et al., *Quat. Res.* **14**, 309 (1980).
9. E. L. Sikes and L. D. Keigwin, *Paleoceanography* **9**, 31 (1994); A. C. Mix, W. F. Ruddiman, A. McIntyre, *Paleoceanography* **1**, 43 (1986); A. C. Mix, W. F. Ruddiman, A. McIntyre, *Paleoceanography* **1**, 339 (1986); R. Schneider, P. J. Mueller, G. Ruhland, *Paleoceanography* **10**, 197 (1995).
10. E. Bard, F. Rostek, C. Sonzogni, *Nature* **385**, 707 (1997); F. Rostek et al., *Nature* **364**, 319 (1993).
11. The $\delta^{18}\text{O}$ notation is

$$\delta^{18}\text{O} = \left[\frac{(^{18}\text{O}/^{16}\text{O})_{\text{sample}}}{(^{18}\text{O}/^{16}\text{O})_{\text{std}}} - 1 \right] \times 1000$$
 where std is the standard mean ocean water reference.
12. T. P. Guilderson, R. G. Fairbanks, J. L. Rubenstone, *Science* **263**, 663 (1994); J. W. Beck et al., *Science* **257**, 644 (1992); J. W. Beck, J. Récy, F. Taylor, R. L. Edwards, G. Cabioch, *Nature* **385**, 705 (1997).
13. C. M. Clapperton, *Palaeogeogr. Palaeoclimatol. Palaeoecol.* **101**, 189 (1993).
14. P. Webster and N. Stretten, *Quat. Res.* **10**, 279 (1978); D. Rind and D. Peteet, *Quat. Res.* **24**, 1 (1985).
15. M. B. Bush, P. A. Colinvaux, M. C. Wieman, D. R. Piperno, K. b. Liu, *Quat. Res.* **34**, 330 (1990); M. B. Bush et al., *Ecol. Monogr.* **62**, 251 (1992).
16. B. W. Leyden, M. Brenner, D. A. Hodell, J. H. Curties, in *Climate Change in Continental Isotopic Records*, vol. 78 of *Geophysical Monograph Series*, P. K. Swart, K. C. Lohmann, J. McKenzie, S. Savin, Eds. (American Geophysical Union, Washington, DC, 1993), pp. 156–178; K. b. Liu and P. A. Colinvaux, *Nature* **318**, 556 (1985).
17. L. G. Thompson et al., *Science* **269**, 46 (1995); L. G. Thompson et al., *Science* **282**, 1858 (1998).
18. R. T. Pierrehumbert, *Geophys. Res. Lett.* **26**, 1345 (1999).
19. M. Stute et al., *Science* **269**, 379 (1995).
20. M. Stute and A. S. Talma, in *Isotope Techniques in the Study of Environmental Change* (International Atomic Energy Agency, Vienna, 1998), pp. 307–318; W. M. Edmunds, E. Fellman, I. B. Goni, G. McNeill, D. D. Harkness, in *Isotope Techniques in the Study of Environmental Change* (International Atomic Energy

- Agency, Vienna, 1998), pp. 693–707; W. M. Edmunds, E. Fellman, I. B. Goni, *J. Geol. Soc. London* **156**, 345 (1999).
21. E. Mazor, *Geochim. Cosmochim. Acta* **36**, 1321 (1972); M. Stute and P. Schlosser, in *Climate Change in Continental Isotopic Records*, vol. 78 of *Geophysical Monograph Series*, P. K. Swart, K. C. Lohmann, J. McKenzie, S. Savin, Eds. (American Geophysical Union, Washington, DC, 1993), pp. 89–100.
22. The $\delta^2\text{H}$ notation is

$$\delta^2\text{H} = \left[\frac{(^2\text{H}/^1\text{H})_{\text{sample}}}{(^2\text{H}/^1\text{H})_{\text{std}}} - 1 \right] \times 1000$$
 where std is the standard mean ocean water reference.
23. W. Dansgaard, *Tellus* **16**, 436 (1964); K. Rozanski, L. Araguás-Araguás, R. Gonfiantini, *Science* **258**, 981 (1992); in *Climate Change in Continental Isotopic Records*, vol. 78 of *Geophysical Monograph Series*, P. K. Swart, K. C. Lohmann, J. McKenzie, S. Savin, Eds. (American Geophysical Union, Washington, DC, 1993), pp. 1–36.
24. S. Hastenrath, *Climate and Circulation of the Tropics* (Reidel, Dordrecht, Netherlands, 1985).
25. D. E. Pedgely, *Weather* **24**, 456 (1969); *Meteorol. Mag.* **99**, 29 (1970).
26. C. E. Weyhenmeyer, S. J. Burns, H. N. Waber, A. Matter, unpublished data.
27. Groundwater residence times were calculated by correcting measured ^{14}C values for chemical reactions along the groundwater flow path (i.e., soil CO_2 exchange and mineral dissolution and precipitation) with the mass balance code NETPATH version 2.0 [L. N. Plummer, E. C. Prestemon, D. L. Parkhurst, *U.S. Geol. Surv. Water Resour. Invest. Rep.* **94-4169** (1994)].
28. M. Stuiver et al., *Radiocarbon* **40**, 1041 (1998).
29. In the inverse method to determine NGT, models describing the concentrations of atmospheric noble gases He (not used in this study), Ne, Ar, Kr, and Xe by the temperature-dependent solubility equilibrium concentrations plus a possibly fractionated excess air component are inverted to obtain the best estimates for the model parameters, including temperature [W. Aeschbach-Hertig, F. Peeters, U. Beyerle, R. Kipfer, *Water Resour. Res.* **35**, 2779 (1999)]. Recently, C. J. Ballentine and C. M. Hall [*Geochim. Cosmochim. Acta*

- 63**, 2315 (1999)] used the inverse approach to show that available excess air models are insufficient to describe the fractionation observed in the noble gas records from several locations, including Brazil (79). This described problem is overcome by a model explaining excess air fractionation by equilibration of groundwater with entrapped air (W. Aeschbach-Hertig, F. Peeters, U. Beyerle, R. Kipfer, unpublished data). This model yields good fits for nine samples from Oman. Two samples cannot be described by any currently known model, and hence no NGT could be calculated (30).
30. See supplementary table available at www.sciencemag.org/feature/data/1045634.shl.
31. F. Sirocko et al., *Nature* **364**, 322 (1993).
32. S. C. Clemens, W. Prell, D. Murray, G. Shimmiel, G. Weedon, *Nature* **353**, 720 (1991).
33. F. Sirocko, M. Sarnthein, H. Lange, H. Erlenkeuser, *Quat. Res.* **36**, 72 (1991).
34. Because of the temperature dependence of fractionation processes, the glacial-interglacial temperature increase of 6.5°C should be reflected by more negative $\delta^{18}\text{O}$ and $\delta^2\text{H}$ values in the Late Pleistocene groundwater compared with modern groundwater. In the low latitudes, however, the $\delta^{18}\text{O}$ signal appears to be more affected by the amount and source of precipitation rather than by temperature [J. R. Lawrence and S. D. Gedzelman, *Geophys. Res. Lett.* **23**, 527 (1996)].
35. E. Van Campo, *Quat. Res.* **26**, 376 (1986).
36. F. A. Street and A. T. Grove, *Quat. Res.* **12**, 83 (1979).
37. F. Gasse, R. Tehet, A. Durand, E. Gilbert, J. C. Fontes, *Nature* **346**, 141 (1990).
38. S. Burns, A. Matter, N. Frank, A. Mangini, *Geology* **26**, 499 (1998).
39. R. G. Fairbanks, *Nature* **342**, 637 (1989).
40. We thank the Ministry of Water Resources (MWR) of the Sultanate of Oman for their permission to conduct this fieldwork as well as for their logistic and scientific support; Z. Al Suleimani, former Director of Research, and P. Macumber, former Head of the Groundwater Section, MWR, for their assistance during various stages of this project; and U. Beyerle and S. Reese for their laboratory work.

22 September 1999; accepted 10 December 1999

Cross-Species Interactions Between Malaria Parasites in Humans

Marian C. Bruce,^{1*} Christl A. Donnelly,¹ Michael P. Alpers,² Mary R. Galinski,³ John W. Barnwell,⁴ David Walliker,⁵ Karen P. Day¹

The dynamics of multiple *Plasmodium* infections in asymptomatic children living under intense malaria transmission pressure provide evidence for a density-dependent regulation that transcends species as well as genotype. This regulation, in combination with species- and genotype-specific immune responses, results in nonindependent, sequential episodes of infection with each species.

In malaria-endemic regions, humans commonly harbor chronic *Plasmodium* infections consisting of complex mixtures of different species (1) and genotypes of parasites (2). Longitudinal studies of animal malaria infections have shown that infection dynamics are affected by cross-species immunity, resulting in within-host interactions between species [reviewed in (3)]. Direct evidence for the action of cross-species immunity in human

malaria infections has been lacking. Consecutive experimental infections with different species and genotypes indicated that immunity to human malaria is species- and genotype-specific (4). Data on the dynamics of simultaneous multispecies (5) and multigenotype coinfections (6) are available from only a few experiments. In some instances of mixed infections of *P. falciparum* and *P. vivax*, replacement of one species with another